

Backtracking activation impacts the criticality of excitable networks

Renquan Zhang and Guoyi Quan

School of Mathematical Sciences, Dalian University of Technology, Dalian 116024, China

Jiannan Wang*

Research Institute of Frontier Science,

Beihang University, Beijing 100191, China

Key Laboratory of Mathematics Informatics

Behavioral Semantics, Ministry of Education, China

Sen Pei[†]

Department of Environmental Health Sciences, Mailman School of Public Health,

Columbia University, New York, NY 10032, USA

Abstract

Networks of excitable elements are widely used to model real-world biological and social systems. The dynamic range of an excitable network quantifies the range of stimulus intensities that can be robustly distinguished by the network response, and is maximized at the critical state. In this study, we examine the impacts of backtracking activation on system criticality in excitable networks consisting of both excitatory and inhibitory units. We find that, for dynamics with refractory states that prohibit backtracking activation, the critical state occurs when the largest eigenvalue of the weighted non-backtracking (WNB) matrix for excitatory units, λ_{NB}^E , is close to one, regardless of the strength of inhibition. In contrast, for dynamics without refractory state in which backtracking activation is allowed, the strength of inhibition affects the critical condition through suppression of backtracking activation. As inhibitory strength increases, backtracking activation is gradually suppressed. Accordingly, the system shifts continuously along a continuum between two extreme regimes – from one where the criticality is determined by the largest eigenvalue of the weighted adjacency matrix for excitatory units, λ_W^E , to the other where the critical state is reached when λ_{NB}^E is close to one. For systems in between, we find that $\lambda_{NB}^E < 1$ and $\lambda_W^E > 1$ at the critical state. These findings, confirmed by numerical simulations using both synthetic and realistic networks, indicate that backtracking activation impacts the criticality of excitable networks. This result can be generalized to other dynamical processes with backtracking activation such as certain epidemic spread and information diffusion models.

Keywords: excitable networks, criticality, backtracking activation, non-backtracking matrix, excitatory-inhibitory networks, dynamic range

* wangjiannan@buaa.edu.cn

† sp3449@cumc.columbia.edu

1. INTRODUCTION

Excitable networks have been used to model a range of phenomena in biological and social systems including signal propagation in neural networks [1–6], information processing in brain networks [7–9], epidemic spread in human population and information diffusion in social networks [10–13]. The collective dynamics of excitable nodes enable the networked system to distinguish stimulus intensities varied by several orders of magnitude, characterized by a large dynamic range in response to external stimuli. In previous studies, it was found that, for a number of excitable network models, the dynamic range is maximized at the critical state [1, 14–17]. As a result, understanding the condition of criticality is essential for improving the performance and functionality of excitable networks.

The critical condition for excitable networks composed of only excitatory nodes has been extensively studied. In homogeneous random networks, the critical state corresponds to a unit branching ratio [1]. For more general network structures, the criticality for dynamics without refractory state is characterized by the unit largest eigenvalue of the weighted adjacency matrix [14]. More recently, it was shown that for dynamics with refractory states, the critical state is governed by the largest eigenvalue of the weighted non-backtracking (WNB) matrix [17]. In these studies, the largest eigenvalue of the weighted adjacency matrix or WNB matrix is used to define the critical state of excitable networks. However, when inhibitory nodes are introduced, it is unclear how criticality is related to the largest eigenvalues of these two matrices.

In this study, we explore the critical condition of excitable networks consisting of both excitatory (E) and inhibitory (I) nodes. Inhibition presents in many real-world systems and plays a critical role in model dynamics and functions [18–23]. For instance, the introduction of inhibitory nodes into an excitable network operating near the critical state leads to self-sustained network activity [22], and inhibitory connectivity may be essential in maintaining long-term information storage in volatile cortex [23]. In order to elucidate the relationship between criticality and the largest eigenvalues of the weighted adjacency matrix and WNB matrix, we study an excitatory-inhibitory (EI) network model equipped with a threshold-like activation rule [22]. Specifically, we focus on the impact of backtracking activation paths on the critical condition.

We first analyze the model dynamics of EI networks in two extreme conditions where

backtracking activation is allowed without restrictions or entirely prohibited. We find that, in the former case, the critical state is better characterized by the largest eigenvalue of the weighted adjacency matrix for excitatory nodes, λ_W^E , while in the latter case, the criticality is more related to the largest eigenvalue of the WNB matrix for excitatory nodes, λ_{NB}^E . For EI models with refractory states that preclude backtracking activation, the critical state is achieved when λ_{NB}^E is close to one. For EI models without refractory state (i.e., with only resting and excited states), however, the analytical form of the critical condition becomes intractable. We show that, qualitatively, the system gradually shifts from the former case to the latter case as the strength of inhibition increases: for negligible inhibition, λ_W^E is closer to one at the critical state; for strong inhibition, λ_{NB}^E is closer to one at the critical state; for moderate inhibition, we find $\lambda_{NB}^E < 1$ and $\lambda_W^E > 1$ at the critical state. Using numerical simulations in both synthetic and realistic networks, we verify that a larger inhibitory strength tends to suppress more backtracking activation, which explains the transition between these two regimes. Our findings highlight the impact of backtracking activation, a form of dynamical resonance, on the criticality of excitable networks, and may provide new insight into the study of similar dynamical processes in networked systems.

2. MATERIALS AND METHODS

A. The excitable network model

We consider excitable networks consisting of both excitatory (E) and inhibitory (I) nodes [22]. Contrary to the function of excitatory nodes, the effect of inhibitory nodes is to decrease the activation probability of their neighbors once they are activated. In a network with N nodes, we use $s_i(t)$ to represent the state of node i at time t . Both types of nodes can be in one of $m + 1$ states: the resting state $s_i(t) = 0$, the excited state $s_i(t) = 1$, and refractory states $s_i(t) = 2, 3, \dots, m$. At each discrete time t , a resting node can be activated by an external stimulus with a probability η , or activation propagation from its neighbors independently. Specifically, the signal input strength from a node j to a neighboring node i , denoted by a_{ij} , satisfies $a_{ij} > 0$ if node j is excitatory and $a_{ij} < 0$ if node j is inhibitory. If node j and node i are not connected in the network, we set $a_{ij} = 0$. The weighted adjacency matrix $A = \{a_{ij}\}_{N \times N}$ thus fully describes the network structure as well

as the signal input strength between all pairs of nodes. If a resting node i is not activated by the external stimulus, its activation probability in the next time step $t + 1$ is calculated by summing inputs from all neighbors through a transfer function $\sigma(\cdot)$:

$$s_i(t + 1) = 1 \text{ with probability } \sigma \left(\sum_{j=1}^N a_{ij} \tau(s_j(t)) \right). \quad (1)$$

Here $\sigma(\cdot)$ is a piecewise linear function: $\sigma(x) = 0$ for $x \leq 0$; $\sigma(x) = x$ for $0 < x < 1$; and $\sigma(x) = 1$ for $x \geq 1$. $\tau(\cdot)$ is a characteristic function: when $s_j(t) = 1$, $\tau(s_j(t)) = 1$, otherwise, $\tau(s_j(t)) = 0$. A node can be activated by its neighbors if the net input is positive. Once activated, node i will transit to refractory states deterministically. That is, $s_i(t+1) = s_i(t)+1$ if $1 \leq s_i(t) < m$ and $s_i(t+1) = 0$ if $s_i(t) = m$. Note that, if $m = 1$, there will be no refractory state and the node will directly return to the resting state after activation.

In this study, we use *undirected* networks in which signals can be transmitted in both directions, and assume that the number of E nodes N_e is larger than the number of I nodes N_i . For ease of analysis, we rearrange node indices so that nodes with index $1 \leq i \leq N_e$ are excitatory and the rest are inhibitory. We consider both homogeneous and heterogeneous networks. For homogeneous network structure, we first generate two Erdős-Rényi (ER) random networks consisting of N_e excitatory nodes and N_i inhibitory nodes. Within each network, each pair of nodes is connected with a probability α . We then randomly connect E nodes and I nodes with a probability β . For heterogeneous network structure, two scale-free (SF) networks of E nodes and I nodes with a power-law degree distribution $P(k) \propto k^{-\gamma}$ are generated using the configuration model [24]. These two networks are then connected by randomly linking E nodes and I nodes with a probability β . We assume the absolute values of link weights $|a_{ij}|$ are distributed uniformly within a range, and the effect of inhibitory nodes is solely represented by the connections between E and I nodes. By tuning the cross-type linking probability β , we can adjust the inhibitory strength in the EI network.

B. Dynamic range and criticality

The dynamic range of an excitable network measures the range of stimulus intensities that are distinguishable based on network response [1]. For a given stimulus intensity $\eta \in (0, 1)$,

the network response F is defined as

$$F = \lim_{T \rightarrow \infty} \frac{1}{T} \sum_{t=0}^T S^t, \quad (2)$$

where S^t is the fraction of excited nodes at time t . The response $F(\eta)$ increases monotonically with a growing intensity of external stimulus η in a nonlinear fashion (see figure 1). For a strong stimulus intensity $\eta \rightarrow 1$, the response $F(\eta)$ will saturate and retain at a maximum value $F_{max} = 1/(m + 1)$. For a negligible stimulus intensity $\eta \rightarrow 0$, the minimum response F_0 depends on the state of the excitable system. In subcritical state, $F(\eta)$ is a linear function of η for $\eta \rightarrow 0$, i.e., $F(\eta) \propto \eta$, with $F_0 \rightarrow 0$. At the critical state, F_0 still approaches to zero but the function $F(\eta)$ becomes nonlinear: $F(\eta) \propto \eta^{1/2}$ (see figure 1(a)). The exponent $1/2$ is called the Steven's exponent, which characterizes the criticality of the collective dynamics [1, 25]. In supercritical state, the excitation caused by external stimulus can be self-sustained. Therefore, F_0 becomes a positive number.

The dynamic range of an excitable network is defined based on the function $F(\eta)$. In particular, we define dynamic range Δ as

$$\Delta = 10 \log_{10} \frac{\eta_{high}}{\eta_{low}}, \quad (3)$$

where η_{high} and η_{low} are stimulus intensities corresponding to network responses F_{high} and F_{low} (here $F_x = F_0 + x(F_{max} - F_0)$ for $x \in [0, 1]$). In this study, we use $\eta_{0.9}$ and $\eta_{0.1}$, discarding stimuli that are too close to saturation or too weak to be distinguished from F_0 . Previous studies have demonstrated that dynamic range is maximized at the critical state of an excitable system [1, 14]. Without forcing of external stimuli, excitation activity will eventually die out in subcritical state but become self-sustained above the critical point. This feature allows us to identify the critical point using the maximization of dynamic range.

3. RESULTS

The number of refractory states in model dynamics determines whether backtracking activation is permitted. Backtracking activation describes the following phenomenon of dynamical resonance: an excitatory node i activated at time t increases the activation probability of its excitatory neighbors at time $t + 1$, which in turn increases the activation probability of node i at time $t + 2$. This behavior is only possible when there is no refractory

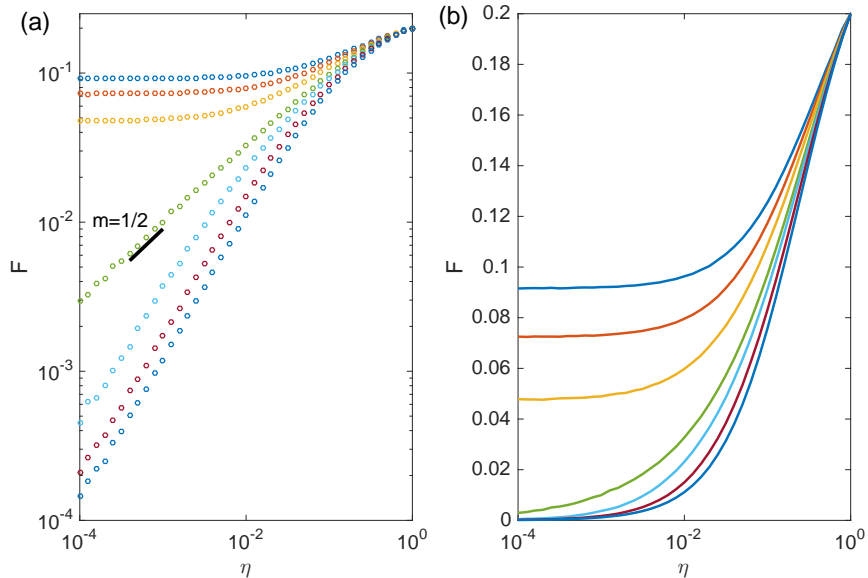


FIG. 1. Network response F in response to external stimulus intensity η . We show the response curves for an EI network constructed by connecting two ER networks ($N_e = 3,000$, $N_i = 2,000$, $\alpha = 3 \times 10^{-3}$, $\beta = 1 \times 10^{-3}$, $m = 4$). The absolute link weights $|a_{ij}|$ are drawn uniformly from 0.1 to 0.2. We multiply link weights with different values to adjust the system to stay in the subcritical, critical and supercritical states. The network response F is shown in logarithmic scale in (a) and linear scale in (b). At the critical state, we show that $F(\eta) \propto \eta^{1/2}$ in (a). The dynamic range of the system is calculated based on the response curve.

state (i.e., $m = 1$) so that excited nodes can directly return to the resting state at time $t + 1$. For dynamics with refractory states (i.e., $m > 1$), nodes excited at time t will enter refractory states at time $t + 1$ thus cannot be activated again at time $t + 2$. Following this dynamical rule, any backtracking activation is prohibited.

A. Dynamics without backtracking activation

We first analyze the simpler case where backtracking is precluded by the existence of refractory states (i.e., $m > 1$). To account for the dynamics without backtracking, we formulate the model evolution in a message-passing framework [17], which is frequently used in statistical physics and network science [26–28]. For a link from i to j ($i \rightarrow j$), we create a “cavity” at node j by “virtually” removing it from the network, and examine the

probability of node i being activated in the absence of node j , denoted by $p_{i \rightarrow j}^t$ at time t . The procedure of creating a virtual cavity at node j blocks the backtracking path $i \rightarrow j \rightarrow i$, and therefore excludes the contribution via the consecutive activation $i \rightarrow j \rightarrow i$ to the activation probability of node i . This framework precisely depicts the model dynamics with refractory states.

For sparse networks without too many short loops, the probabilities $p_{i \rightarrow j}^t$ for neighboring nodes are mutual independent. Under this condition, the probability $p_{i \rightarrow j}^t$ for each node i can be recursively written as follows:

$$p_{i \rightarrow j}^{t+1} = \left(1 - \sum_{l=0}^{m-1} p_{i \rightarrow j}^{t-l}\right) \left[\eta + (1 - \eta) \sigma \left(\sum_{k \in \partial i \setminus j} a_{ik} p_{k \rightarrow i}^t \right) \right]. \quad (4)$$

Here $\partial i \setminus j$ is the set of neighbors of node i excluding j . The probability that node i is excited at time $t + 1$, denoted by p_i^{t+1} , is calculated by putting node j back to the network:

$$p_i^{t+1} = \left(1 - \sum_{l=0}^{m-1} p_i^{t-l}\right) \left[\eta + (1 - \eta) \sigma \left(\sum_{k \in \partial i} a_{ik} p_{k \rightarrow i}^t \right) \right]. \quad (5)$$

Note that, although Eqs (4)-(5) are derived for locally tree-like sparse networks, it has been found that results based on the sparseness assumption work well even for some networks with dense clusters [29].

1. Analysis in the case of negligible inhibition

The piecewise transfer function $\sigma(\cdot)$ imposes a threshold-like activation rule that depends on the collective dynamics of all neighbors. Because the value of net input $\sum_{k \in \partial i \setminus j} a_{ik} p_{k \rightarrow i}^t$ is unknown, it becomes complicated to expand the right-hand-side of Eq (4) except for some extreme cases. Here, we consider a special case where the cross-type interaction β is negligible, i.e., $\beta \rightarrow 0$. Under this extreme condition, excitatory and inhibitory nodes in effect form two nearly separate communities. In particular, inhibitory nodes are unlikely to be activated in response to weak stimuli as they almost only receive signals from inhibitory peers. As a consequence, it is suffice to consider only excitatory nodes to compute network response.

In the steady state, denote the limiting probabilities as $\lim_{t \rightarrow \infty} p_{i \rightarrow j}^t = p_{i \rightarrow j}$ and $\lim_{t \rightarrow \infty} p_i^t =$

p_i . For excitatory nodes, Eqs (4)-(5) becomes

$$p_{i \rightarrow j} = (1 - mp_{i \rightarrow j}) \left[\eta + (1 - \eta) \sum_{k \in \partial_E i \setminus j} a_{ik} p_{k \rightarrow i} \right], \quad (6)$$

$$p_i = (1 - mp_i) \left[\eta + (1 - \eta) \sum_{k \in \partial_E i} a_{ik} p_{k \rightarrow i} \right], \quad (7)$$

where $1 \leq i \leq N_e$, $1 \leq j \leq N_e$ and $\partial_E i$ is the set of excitatory neighbors of node i . To solve the self-consistent equations, we introduce two auxiliary variables: $G_{i \rightarrow j}(\eta, p_{\rightarrow}) = \eta + (1 - \eta) \sum_{k \in \partial_E i \setminus j} a_{ik} p_{k \rightarrow i}$, $G_i(\eta, p_{\rightarrow}) = \eta + (1 - \eta) \sum_{k \in \partial_E i} a_{ik} p_{k \rightarrow i}$. We rearrange Eqs (6)-(7) and obtain

$$p_{i \rightarrow j} = \frac{G_{i \rightarrow j}(\eta, p_{\rightarrow})}{mG_{i \rightarrow j}(\eta, p_{\rightarrow}) + 1} \quad (8)$$

and

$$p_i = \frac{G_i(\eta, p_{\rightarrow})}{mG_i(\eta, p_{\rightarrow}) + 1}. \quad (9)$$

For $\eta = 0$ (that is, without external forcing), Eq (8) has a trivial solution: $p_{i \rightarrow j} = 0$ for all links $i \rightarrow j$. The stability of this solution determines the critical state of the system. If the solution is stable, the network activity triggered by a weak stimulus will eventually disappear; otherwise, the response will maintain at a nonzero level.

The stability of the zero solution depends on the Jacobian matrix $\widehat{\mathcal{M}}^E = \{\mathcal{M}_{k \rightarrow l, i \rightarrow j}^E\}$ defined on all pairs of links $k \rightarrow l$ and $i \rightarrow j$ between E nodes. Specifically, we have

$$\begin{aligned} \mathcal{M}_{k \rightarrow l, i \rightarrow j}^E &= \left. \frac{\partial p_{i \rightarrow j}}{\partial p_{k \rightarrow l}} \right|_{\{\eta=0, p_{i \rightarrow j}=0\}} \\ &= \frac{\frac{\partial G_{i \rightarrow j}}{\partial p_{k \rightarrow l}} (mG_{i \rightarrow j} + 1) - mG_{i \rightarrow j} \frac{\partial G_{i \rightarrow j}}{\partial p_{k \rightarrow l}}}{(mG_{i \rightarrow j} + 1)^2} \\ &= \left. \frac{\partial G_{i \rightarrow j}}{\partial p_{k \rightarrow l}} \right|_{\{\eta=0, p_{i \rightarrow j}=0\}}. \end{aligned} \quad (10)$$

Here $G_{i \rightarrow j} = 0$ when $\eta = 0$ and $p_{i \rightarrow j} = 0$ for all $i \rightarrow j$. According to the definition of $G_{i \rightarrow j}$, the partial derivative of $G_{i \rightarrow j}$ is given by

$$\left. \frac{\partial G_{i \rightarrow j}}{\partial p_{k \rightarrow l}} \right|_{\{\eta=0, p_{i \rightarrow j}=0\}} = \begin{cases} a_{lk} & \text{if } l = i \text{ and } j \neq k, \\ 0 & \text{otherwise.} \end{cases} \quad (11)$$

The elements of $\widehat{\mathcal{M}}^E$ are $\mathcal{M}_{k \rightarrow l, i \rightarrow j}^E = a_{lk}$ if $l = i$ and $j \neq k$ and 0 otherwise. Note that, $\mathcal{M}_{k \rightarrow l, i \rightarrow j}^E$ is non-zero only if the links $k \rightarrow l$ and $i \rightarrow j$ are consecutive ($l = i$) but

not backtracking ($j \neq k$). The weighted non-backtracking (WNB) matrix, or Hashimoto matrix [30], has recently found applications in several problems in network science [27, 31–36]. Because the stability of the zero solution is determined by the largest eigenvalue λ_{NB}^E of $\widehat{\mathcal{M}}^E$, the system reaches the critical state if $\lambda_{NB}^E = 1$.

2. Numerical results for dynamics with inhibition

For the general case where inhibition cannot be neglected, it is challenging to derive the analytical condition of criticality from Eq (4). As a result, we have to use numerical methods to find the critical state. In particular, we are interested in how the largest eigenvalue of the WNB matrix for E nodes λ_{NB}^E changes with the inhibitory strength β at the critical state. We treat the increasing level of inhibition as a perturbation to the special case of $\beta = 0$, and examine to what extent the critical condition $\lambda_{NB}^E = 1$ will remain valid. In order to tune the system to the critical state, for a fixed inhibitory strength β , we randomly draw absolute link weights $|a_{ij}|$ from a uniform distribution between 0.1 and 0.2, and then multiply $|a_{ij}|$ with a varying constant until the dynamic range of the system is maximized (i.e., the critical state is reached). The largest eigenvalue λ_{NB}^E of $\widehat{\mathcal{M}}^E$ is then computed using a power method [37]. In figure 2, we show the relationship between dynamic range and the largest eigenvalues of four matrices (i.e., the weighted adjacency matrix for all nodes, the weighted non-backtracking matrix for all nodes, the weighted adjacency matrix for E nodes, and the weighted non-backtracking matrix for E nodes). The curves present the largest eigenvalues of different matrices at the critical state where dynamic range is maximized.

We first analyze homogeneous network structure. Without loss of generality, we assume there are 3 refractory states ($m = 4$). For ER networks with $N_e = 3,000$ excitatory nodes and $N_i = 2,000$ inhibitory nodes, we set the within-type connection probability $\alpha = 3 \times 10^{-3}$. An increasing level of inhibitory strength $\beta = 1 \times 10^{-4}, 5 \times 10^{-4}, 1 \times 10^{-3}, 2 \times 10^{-3}$ and 3×10^{-3} are tested. For each β , we slowly tune the link weights to drive the system to the critical state, and record the largest eigenvalue of the WNB matrix for E nodes λ_{NB}^E . We perform 300 realizations of this procedure, and report the distributions of λ_{NB}^E in figure 3. For comparison, we also computed the largest eigenvalue of the weighted adjacency matrix for E nodes λ_W^E at criticality.

Interestingly, even with non-negligible inhibition, λ_{NB}^E consistently distributes around one

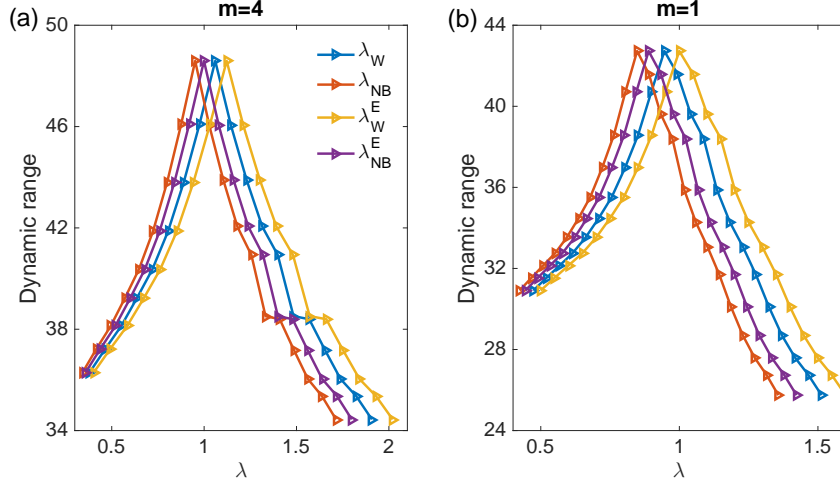


FIG. 2. The relationship between dynamic range and the largest eigenvalues of four matrices for dynamics with 3 refractory states (a) and without refractory state (b). Here, λ_W , λ_{NB} , λ_W^E and λ_{NB}^E are the largest eigenvalues of the weighted adjacency matrix for all nodes, the weighted non-backtracking matrix for all nodes, the weighted adjacency matrix for E nodes, and the weighted non-backtracking matrix for E nodes, respectively. We perform the experiment on an EI network constructed using two ER networks ($N_e = 3,000$, $N_i = 2,000$, $\alpha = 3 \times 10^{-3}$, $\beta = 1 \times 10^{-3}$), and vary link weights to change the state of the system. For each setting of link weights, we calculate the dynamic range and the corresponding largest eigenvalues. The setting that maximizes the dynamic range corresponds to the critical state. We use this numerical method to find the critical state of an EI network. At criticality, we find that λ_{NB}^E is close to one for $m = 4$ and λ_W^E is close to one for $m = 1$. λ_W (λ_{NB}) is always smaller than λ_W^E (λ_{NB}^E) due to the existence of inhibitory nodes.

at the critical state for an increasing inhibitory strength β . In contrast, λ_W^E distributes well above one. We note that the variation of λ_{NB}^E and λ_W^E is attributed to the finite network size and numerical inaccuracy, as pointed out in a previous study on excitable networks with only E nodes [17]. The numerical results in figure 3 indicate that the criticality of EI networks with refractory states occurs when λ_{NB}^E is close to one, regardless of the strength of inhibition β . A closer inspection of figure 3 reveals that the average value of λ_{NB}^E is slighted larger than one and slowly increases with β . This slight shift of λ_{NB}^E indicates that inhibition does impact the critical condition but its impact is very limited.

According to model dynamics, the function of I nodes is passive – they need to be first

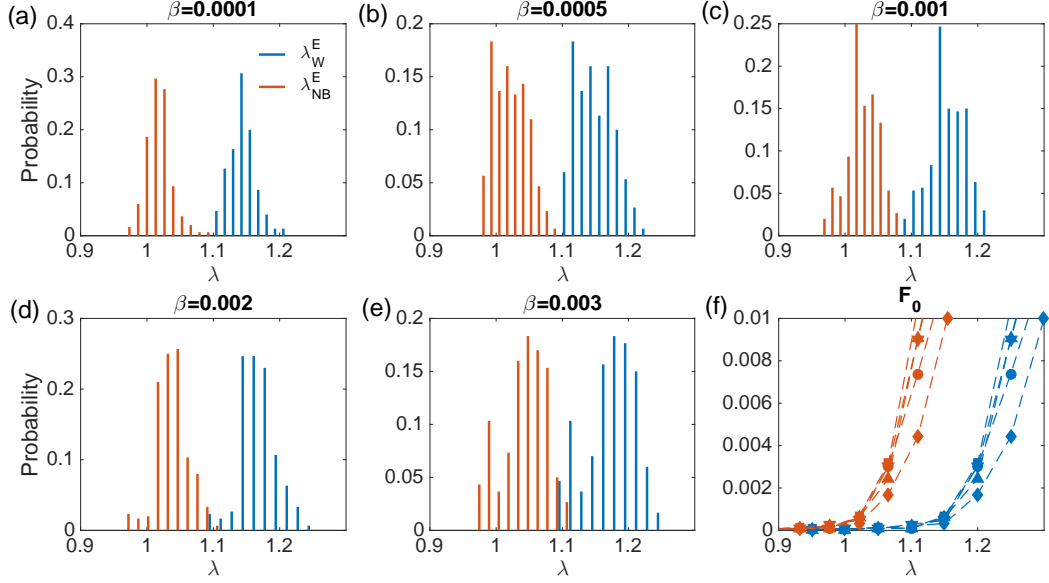


FIG. 3. Distributions of λ_W^E and λ_{NB}^E at the critical state of homogeneous EI networks with refractory states ($m = 4$) (a-e). Networks are constructed by connecting two ER networks ($N_e = 3,000$, $N_i = 2,000$, $\alpha = 3 \times 10^{-3}$), and varying the cross-type link probability β . For different settings of β , λ_{NB}^E is consistently distributed near one. The relationship between F_0 and λ_W^E and λ_{NB}^E is shown in (f) for $\beta = 1 \times 10^{-4}$ (up triangle), 5×10^{-4} (square), 1×10^{-3} (down triangle), 2×10^{-3} (circle), and 3×10^{-3} (diamond). The transition point from $F_0 = 0$ to $F_0 > 0$ is not affected by the strength of inhibition β .

activated before they can release inhibition signals. Without external stimuli, the conduction of inhibitory signals proceeds as follows: a set of excited E nodes activate an I node at time t ; at time $t + 1$, the excited I node exerts inhibitory signals to all its neighbors, among which the excited E nodes enter refractory state. With the presence of nodes in refractory state, we hypothesize that the inhibition effect is weakened. To demonstrate this, we plot F_0 as a function of λ_{NB}^E and λ_W^E for increasing β in figure 3(f). Although the inhibitory strength β intensifies, the F_0 curve does not change significantly, especially near the transition point from $F_0 = 0$ to $F_0 > 0$. This result directly shows that, for dynamics with refractory states, the impact of inhibitory nodes is rather limited near the critical state.

We performed the same analysis in SF networks with $N_e = 6,000$, $N_i = 4,000$ and the power-law exponent $\gamma = 3$. Results in figure 4 show that, consistent with the results for ER networks, λ_{NB}^E is close to one at the critical state. The effect of inhibitory nodes near

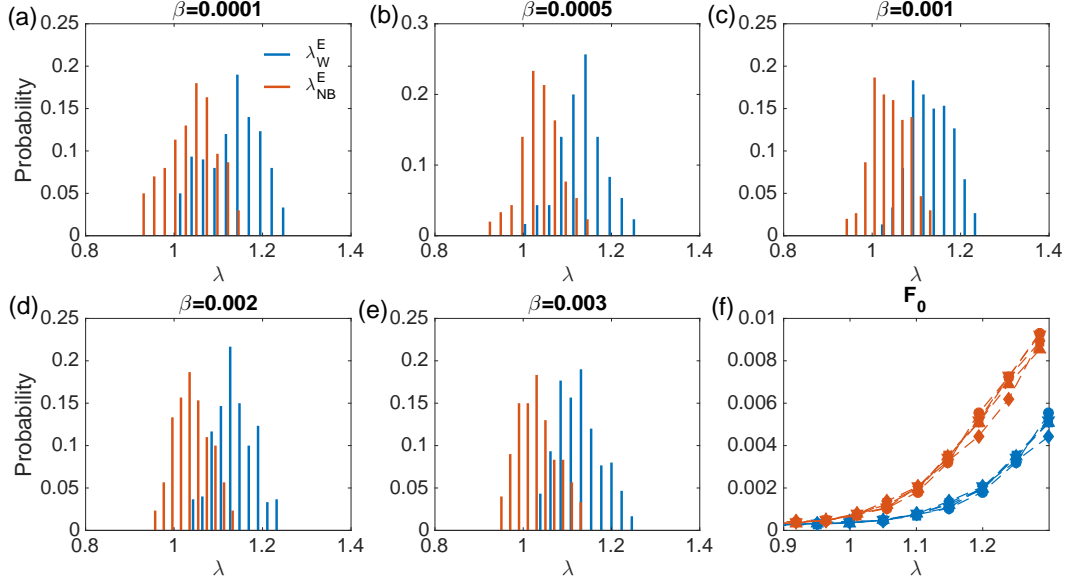


FIG. 4. Distributions of λ_W^E and λ_{NB}^E at the critical state of heterogeneous EI networks with refractory states ($m = 4$) (a-e). Networks are constructed by connecting two SF networks ($N_e = 6,000$, $N_i = 4,000$, $\gamma = 3$), and varying the cross-type link probability β . For different settings of β , λ_{NB}^E is consistently distributed near one. The relationship between F_0 and λ_W^E and λ_{NB}^E is shown in (f) for $\beta = 1 \times 10^{-4}$ (up triangle), 5×10^{-4} (square), 1×10^{-3} (down triangle), 2×10^{-3} (circle), and 3×10^{-3} (diamond). The transition point from $F_0 = 0$ to $F_0 > 0$ is not affected by the strength of inhibition β .

the critical state is also nominal as the F_0 curves are almost identical for different values of inhibitory strength β .

B. Dynamics with backtracking activation

We now explore the more complicated dynamics in which backtracking activation is allowed. In this case, nodes have only two states – resting and excited. For each node i , denote p_i^t as the probability that node i is excited at time t . According to the model dynamics, the evolution of p_i^t is described by

$$p_i^{t+1} = (1 - p_i^t) \left[\eta + (1 - \eta) \sigma \left(\sum_{k=1}^N a_{ik} p_k^t \right) \right]. \quad (12)$$

Backtracking activation is properly represented in Eq (12): if we expand p_k^t on the right-hand-side of Eq (12) in terms of the activation probability at time $t - 1$, p_i^{t+1} becomes explicitly dependent on p_i^{t-1} . This implies, the activation probability of each E node at a given time can contribute to the probability of its re-activation two time-steps later (as long as at least one of its E neighbors are activated), which exactly depicts the effect of backtracking activation.

1. Analysis in the case of negligible inhibition

Similar with our analysis of dynamics with refractory states, we first explore the extreme case where the cross-type linking probability $\beta \rightarrow 0$. In this case, we only consider the network of excitatory nodes. The stationary activation probability $p_i = \lim_{t \rightarrow \infty} p_i^t$ satisfies

$$p_i = (1 - p_i) \left[\eta + (1 - \eta) \sum_{k=1}^{N_e} a_{ik} p_k \right]. \quad (13)$$

Without external stimuli, the system has a trivial solution $p_i = 0$ for $1 \leq i \leq N_e$. The stability of the zero solution is determined by the largest eigenvalue λ_W^E of the weighted adjacency matrix for excitatory nodes $A^E = \{a_{ij}\}_{N_e \times N_e}$. As a result, the critical state is characterized by $\lambda_W^E = 1$ as $\beta \rightarrow 0$.

2. Numerical results for dynamics with inhibition

We perturb the extreme case $\beta \rightarrow 0$ by gradually increasing the cross-type linking probability β , which introduces more inhibitory nodes connected to excitatory nodes. Without refractory states, an “excitatory→inhibitory→excitatory” feedback loop appears: a group of excited E nodes activate an inhibitory node; the excited I node then releases inhibitory signals and decreases the activation probability of the E nodes who just activated it and now returned to the resting state. The inhibitory signals (negative inputs) impose a threshold for the re-activation of those E nodes. As a consequence, contributions from certain backtracking paths may not be realized. This phenomenon is caused by the threshold-like feature of the transfer function $\sigma(\cdot)$. If the contribution of a backtracking path is lower than the threshold imposed by inhibitory nodes, it may never contribute to the activation probability as $\sigma(x) > 0$ only if the net input $x > 0$. Following this line of reasoning, Eq (13) thus over-

estimates the effect of backtracking activation when more inhibitory nodes are connected to excitatory nodes. A stronger inhibitory strength β will suppress more backtracking activations, which drives the dynamics of EI networks closer to the opposite extreme case where backtracking activation is entirely prohibited, described by Eqs (6)-(7).

We therefore hypothesize that, for a weak inhibitory strength β , λ_W^E is close to one at the critical state; whereas for a strong inhibitory strength, λ_{NB}^E is close to one at the critical state. Varying the cross-type linking probability β modulates the system shifting between these two extreme regimes. For an intermediate inhibitory strength β , we hypothesize that $\lambda_{NB}^E < 1$ and $\lambda_W^E > 1$ at the critical state. We verify this hypothesis using numerical simulations in both homogeneous and heterogeneous networks.

We performed the same analysis as in figure 3 and figure 4, except using a different model dynamics with only resting and excited states. The distributions of λ_W^E and λ_{NB}^E at the critical state for ER networks is shown in figure 5. In agreement with our hypothesis, as β increases, λ_W^E shifts from near one to above one, and λ_{NB}^E shifts from below one to near one. The same phenomenon is also observed for SF networks in figure 6. In order to examine the effect of inhibitory nodes, we plot the F_0 curve as a function of λ_W^E and λ_{NB}^E in figure 5(f) and figure 6(f). In contrast to dynamics with refractory states, introduction of more inhibitory links effectively reduces F_0 , thus strongly impacts the critical state of the system. Such impact is reflected by the change of the transition point above which F_0 becomes non-zero.

Ideally, it would be desirable to show that the number of instances of backtracking activation decreases with an increasing inhibitory strength β . However, as the activation of a node is collectively determined by a group of nodes, it is difficult to disentangle such interaction and identify definitively which backtracking path is responsible for the activation. Despite that, the impact of inhibitory nodes can be reflected by the threshold values that they impose on excitatory nodes. We calculate the average input from I nodes to E nodes in ER and SF networks. Specifically, for a given stimulus intensity η , we compute the average input of resting E nodes from their excited inhibitory neighbors at each time step, and then average over all time steps. In figure 7(a) and (c), we show that the average threshold indeed increases monotonically with β . In addition, a stronger external stimulus η leads to a higher average threshold due to a larger number of excited nodes.

We further calculate the fraction of excitatory links connected to resting E nodes whose

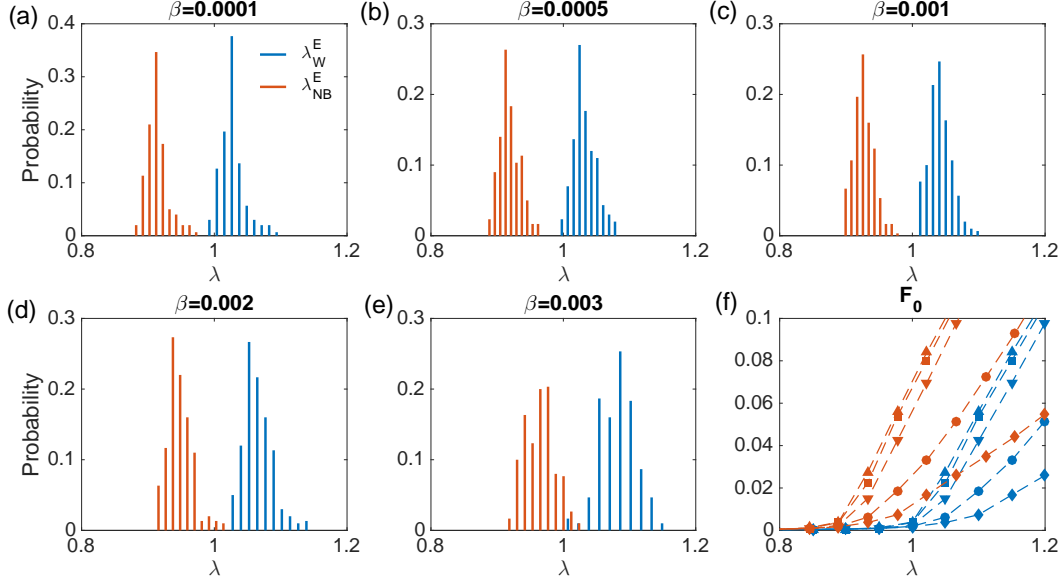


FIG. 5. Distributions of λ_W^E and λ_{NB}^E at the critical state of homogeneous EI networks without refractory state ($m = 1$) (a-e). Networks are constructed by connecting two ER networks ($N_e = 3,000$, $N_i = 2,000$, $\alpha = 3 \times 10^{-3}$), and varying the cross-type link probability β . At the critical state, we show that in general $\lambda_W^E > 1$ and $\lambda_{NB}^E < 1$. As β increases, λ_{NB}^E becomes closer to one and λ_W^E shifts away from one. The relationship between F_0 and λ_W^E and λ_{NB}^E is shown in (f) for $\beta = 1 \times 10^{-4}$ (up triangle), 5×10^{-4} (square), 1×10^{-3} (down triangle), 2×10^{-3} (circle), and 3×10^{-3} (diamond). The transition point from $F_0 = 0$ to $F_0 > 0$ is significantly affected by the strength of inhibition β .

weights are lower than the threshold. To be specific, for each resting E node, we find its excited excitatory neighbors and focus on the links connected to them. These links are potential candidates of backtracking activation, i.e., the actual backtracking activation paths belong to this set of links. Among these links, we calculate the proportion whose weights are lower than the threshold of the E node. The contribution from such below-threshold links are likely to be negated by the threshold. Therefore, the fraction of below-threshold links can partly reflect the magnitude of backtracking suppression. We present an illustration for computing this below-threshold fraction in figure 8. The mean fraction values averaged over all resting E nodes in all time steps for ER and SF networks are shown in figure 7(b) and (d). For both network structures, the fraction of below-threshold links increases as β grows with the presence of different levels of external stimuli. This analysis agrees with our

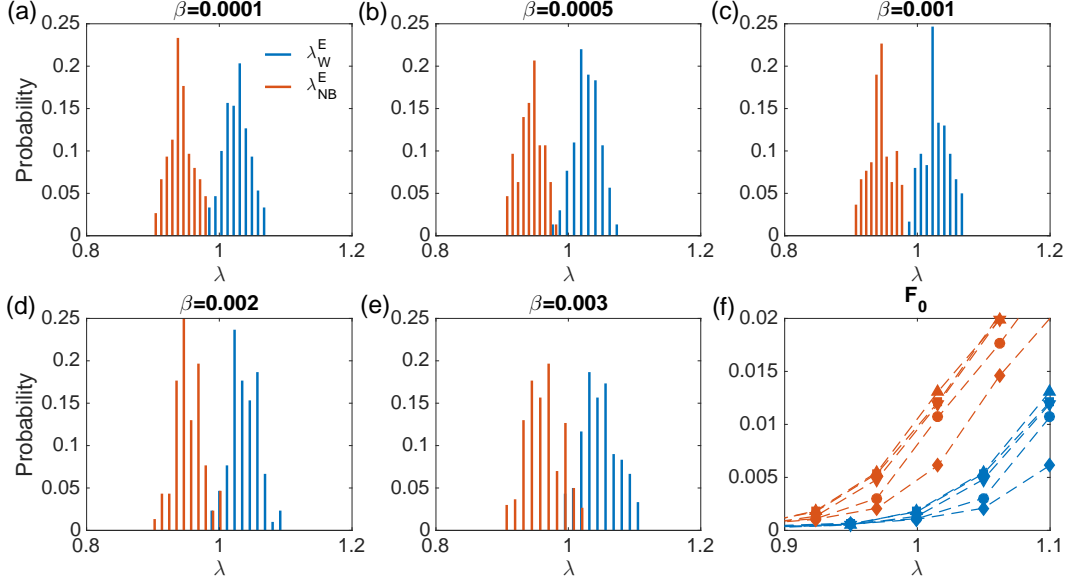


FIG. 6. Distributions of λ_W^E and λ_{NB}^E at the critical state of heterogeneous EI networks without refractory state ($m = 1$) (a-e). Networks are constructed by connecting two SF networks ($N_e = 6,000$, $N_i = 4,000$, $\gamma = 3$), and varying the cross-type link probability β . At the critical state, we show that in general $\lambda_W^E > 1$ and $\lambda_{NB}^E < 1$. As β increases, λ_{NB}^E becomes closer to one and λ_W^E shifts away from one. The relationship between F_0 and λ_W^E and λ_{NB}^E is shown in (f) for $\beta = 1 \times 10^{-4}$ (up triangle), 5×10^{-4} (square), 1×10^{-3} (down triangle), 2×10^{-3} (circle), and 3×10^{-3} (diamond). The transition point from $F_0 = 0$ to $F_0 > 0$ is significantly affected by the strength of inhibition β .

hypothesis and partially explains the transition between the two extreme cases.

C. Simulations in a real-world network

We further validate our findings in real-world networks that have more complex structures. As it is difficult to find a real-world neural network dataset that contains both excitatory and inhibitory neurons, we have to construct an EI network using other types of networks. In particular, we use a human protein interaction network to represent the excitatory network ($N_e = 3,133$ with 6,726 edges) [38], and a yeast protein interaction network to represent the inhibitory network ($N_i = 1,870$ with 2,277 edges) [39]. These two networks are then interconnected by linking E nodes and I nodes with a probability $\beta = 1 \times 10^{-3}$. Note that the network is only used to represent structure with complex features and does

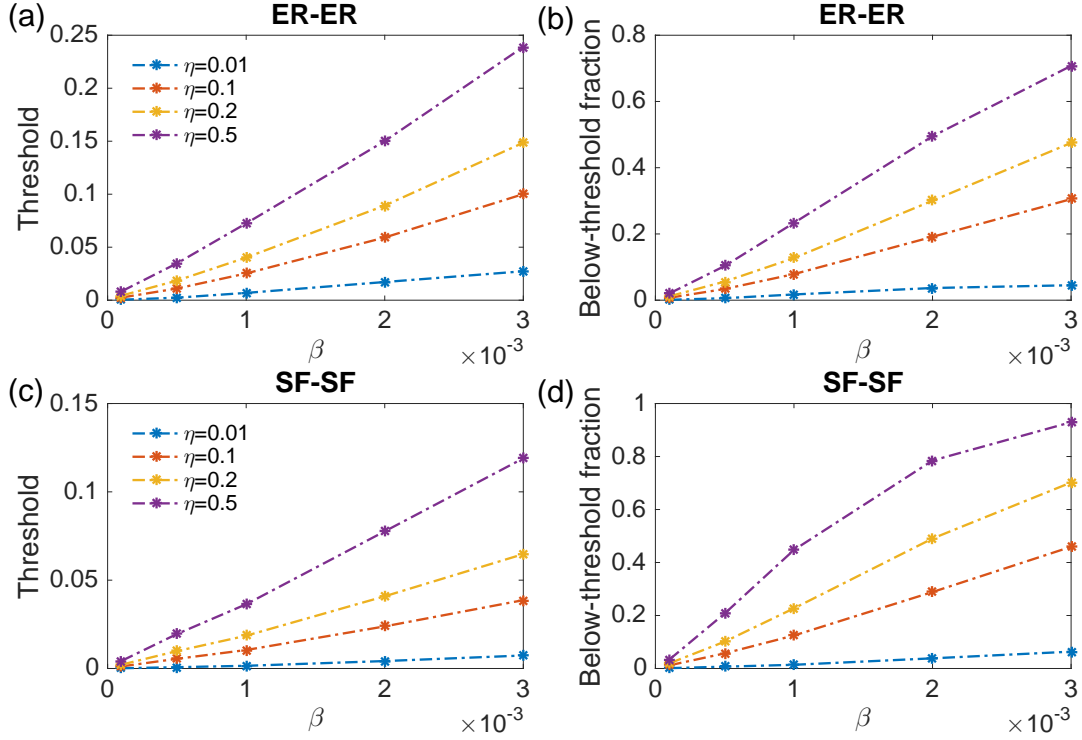


FIG. 7. The threshold of resting E nodes imposed by their inhibitory neighbors for EI networks generated using ER ($N_e = 3,000$, $N_i = 2,000$, $\alpha = 3 \times 10^{-3}$) (a) and SF ($N_e = 6,000$, $N_i = 4,000$, $\gamma = 3$) (c) networks. The fraction of below-threshold links for resting E nodes is reported in (b) and (d). For an increasing level of inhibition strength β , we tune the system to the critical state, and calculate the threshold values and fraction of below-threshold links for different stimulus intensities η . As β and η increase, both threshold and below-threshold fraction increase.

not correspond to any real-world systems. We run simulations of model dynamics without refractory state ($m = 1$). We vary link weights, and calculate the dynamic range, λ_W^E and λ_{NB}^E for each weight setting. The relationship between the dynamic range and λ_W^E and λ_{NB}^E is shown in figure 9. Similar with the results in synthetic networks, at the critical state, we find that $\lambda_W^E > 1$ and $\lambda_{NB}^E < 1$. In the inset, we show the values of λ_W^E and λ_{NB}^E at the critical state for an increasing inhibition strength β . As β grows, at the critical state, λ_W^E shifts away from one and λ_{NB}^E gets closer to one. This result further corroborates our hypothesis that the system lies between two extremes with ($\lambda_W^E \approx 1$) and without ($\lambda_{NB}^E \approx 1$) backtracking activation.

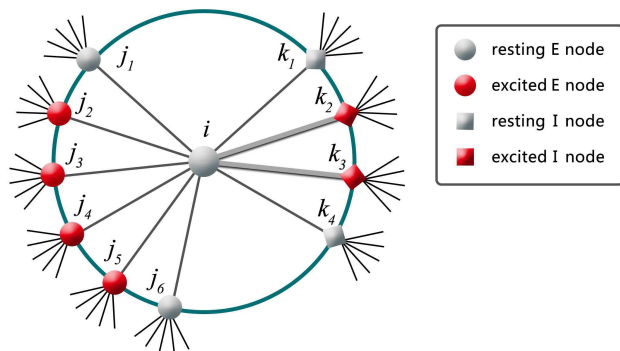


FIG. 8. An example to show the calculation of threshold and fraction of below-threshold links for a resting E node i . Here, the resting E node has a total input $|a_{ik_2} + a_{ik_3}|$ for its activated I neighbors. This value is defined as the threshold. Among the 4 links connected to its activated E neighbors, 2 links have weights below the threshold ($a_{ij_3} < |a_{ik_2} + a_{ik_3}|$, $a_{ij_4} < |a_{ik_2} + a_{ik_3}|$). The fraction of below-threshold links is calculated as $2/4 = 0.5$.

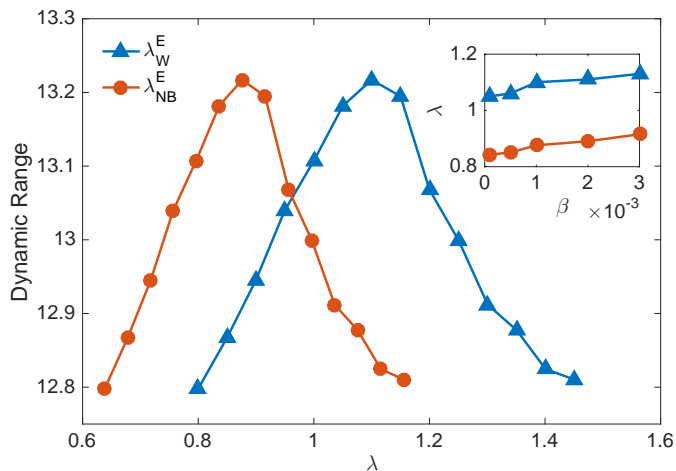


FIG. 9. Relationship between the dynamic range and λ_W^E and λ_{NB}^E for an EI network constructed by connecting two real-world networks ($N_e = 3,133$, $N_i = 1,870$, $\beta = 1 \times 10^{-3}$). We vary link weights to change the state of the system, and calculate the dynamic range, λ_W^E and λ_{NB}^E for each setting. At the critical state where the dynamic range is maximized, we find $\lambda_{NB}^E < 1$ and $\lambda_W^E > 1$, which agrees with our hypothesis. Inset shows the values of λ_W^E and λ_{NB}^E at the critical state for an increasing inhibition strength β .

4. CONCLUSION

In this study, we explore the impact of backtracking activation on the criticality of excitable networks with both excitatory and inhibitory nodes. We find that, for dynamics with refractory state that precludes backtracking activation, the critical state occurs when the largest eigenvalue of the WNB matrix for excitatory nodes is close to one. However, for dynamics without refractory state, the introduction of inhibitory nodes affects backtracking activation and the critical condition of the system. The EI model with inhibition essentially provides an intermediate system between two extreme cases in which backtracking activation is allowed or prohibited. For the dynamics with a medium inhibitory strength, λ_W^E and λ_{NB}^E can be viewed as the upper and lower bound of the critical condition: at the critical state, $\lambda_W^E > 1$ and $\lambda_{NB}^E < 1$. In practice, this criterion can be used to assess whether a system may be at the critical state. If a system resides in a state where $\lambda_W^E < 1$ or $\lambda_{NB}^E > 1$, we can assert that the system is not close to the critical state. Our results imply that a precise description of model dynamics is essential in theoretical analysis of phase transitions. These findings highlight the important role of backtracking activation in spreading dynamics, and could be applied in other dynamical processes with backtracking paths such as the susceptible-infected-susceptible epidemic model.

DATA ACCESSIBILITY

The real-world network data are public available at <http://konect.uni-koblenz.de/networks/maayan> (the human protein interaction network) and http://konect.uni-koblenz.de/networks/moreno_proprio (the yeast protein interaction network).

AUTHORS' CONTRIBUTIONS

All authors designed the study. R.Z. and G.Q. wrote the code, ran simulations and performed the analysis. R.Z., G.Q., J.W. and S.P. wrote, reviewed and edited the manuscript.

COMPETING INTERESTS

We declare we have no competing interests.

FUNDING

This work was supported by the National Natural Science Foundation of China (11801058), the Fundamental Research Funds for the Central Universities (DUT18RC(4)066) and Beijing Natural Science Foundation (1192012, Z180005).

- [1] Kinouchi O and Copelli M 2006 *Nat. Phys.* **2** 348
- [2] Copelli M, Oliveira R F, Roque A C and Kinouchi O 2005 *Neurocomputing* **65** 691
- [3] Gollo L L, Kinouchi O and Copelli M 2009 *PLoS Comput. Biol.* **5** e1000402
- [4] Gollo L L, Copelli M and Roberts J A 2016 *PeerJ* **4** e1912
- [5] Wang C Y, Wu Z X and Chen M Z 2017 *Phys. Rev. E* **95** 012310
- [6] Kinouchi O, Brochini L, Costa A A, Campos J G F and Copelli M 2019 *Sci. Rep.* **9** 3874
- [7] Gautam S H, Hoang T T, McClanahan K, Grady S K and Shew W L 2015 *PLoS Comput. Biol.* **11** e1004576
- [8] Williams-García R V, Moore M, Beggs J M and Ortiz G 2014 *Phys. Rev. E* **90** 062714
- [9] Marro J, Mejias J F, Pinamonti G and Torres J J 2013 *AIP Conference Proceedings* **1510** 85
- [10] Karrer B and Newman M E 2011 *Phys. Rev. E* **84** 036106
- [11] Van Mieghem P 2012 *EPL* **97** 48004
- [12] Dodds P S, Harris K D and Danforth C M 2013 *Phys. Rev. Lett.* **110** 158701
- [13] Pei S, Tang S and Zheng Z 2015 *PLoS ONE* **10** e0124848
- [14] Larremore D B, Shew W L and Restrepo J G 2011 *Phys. Rev. Lett.* **106** 058101
- [15] Larremore D B, Shew W L, Ott E and Restrepo J G 2011 *Chaos* **21** 025117
- [16] Copelli M and Kinouchi O 2005 *Physica A* **349** 431
- [17] Zhang R and Pei S 2018 *Chaos* **28** 013103
- [18] Adini Y, Sagi D and Tsodyks M 1997 *Proc. Natl. Acad. Sci. USA* **94** 10426
- [19] Park C and Terman D 2010 *Chaos* **20** 023122
- [20] Folias S E and Ermentrout G B 2011 *Phys. Rev. Lett.* **107** 228103
- [21] Pei S, Tang S, Yan S, Jiang S, Zhang X and Zheng Z 2012 *Phys. Rev. E* **86** 021909
- [22] Larremore D B, Shew W L, Ott E, Sorrentino F and Restrepo J G 2014 *Phys. Rev. Lett.* **112** 138103

- [23] Mongillo G, Rumpel S and Loewenstein Y 2018 *Nat. Neurosci.* **21** 1463
- [24] Molloy M and Reed B 1995 *Random Struct. Algor.* **6** 161
- [25] Copelli M, Roque A C, Oliveira R F and Kinouchi O 2002 *Phys. Rev. E* **65** 060901
- [26] Mezard M and Montanari A 2009 *Information, Physics, and Computation*(Oxford:Oxford University Press)
- [27] Morone F and Makse H A 2015 *Nature* **524** 65
- [28] Pei S, Teng X, Shaman J, Morone F and Makse H A 2017 *Sci. Rep.* **7** 45240
- [29] Melnik S, Hackett A, Porter M A, Mucha P J and Gleeson J P 2011 *Phys. Rev. E* **83** 036112
- [30] Hashimoto K 1989 *Automorphic Forms and Geometry of Arithmetic Varieties* ed K Hashimoto(Academic Press) pp 211-80
- [31] Martin T, Zhang X and Newman M E 2014 *Phys. Rev. E* **90** 052808
- [32] Karrer B, Newman M E and Zdeborová L 2014 *Phys. Rev. Lett.* **113** 208702
- [33] Hamilton K E and Pryadko L P 2014 *Phys. Rev. Lett.* **113** 208701
- [34] Wang J, Pei S, Wei W, Feng X and Zheng Z 2018 *Phys. Rev. E* **97** 032305
- [35] Wang J, Zhang R, Wei W, Pei S and Zheng Z 2019 *Chaos* **29** 013133
- [36] Aleja D, Criado R, del Amo A J G, Pérez Á and Romance M 2019 *Chaos, Solitons & Fractals* **126** 283
- [37] Saad Y 2011 *Numerical Methods for Large Eigenvalue Problems* (Philadelphia: SIAM)
- [38] Rual J F *et al* 2005 *Nature* **437** 1173
- [39] Coulomb S, Bauer M, Bernard D and Marsolier-Kergoat M C 2005 *Proc. Royal Soc. B* **272** 1721